PROCEEDINGS OF SCIENCE

Semileptonic $D \to \pi \ell \nu$, $D \to K \ell \nu$ and $D_s \to K \ell \nu$ decays with 2+1f domain wall fermions

Peter Boyle,[a,b] **Luigi Del Debbio,**[b] **Felix Erben,**[b] **Jonathan Flynn,**[c] **Andreas Jüttner,**[c,d] **Michael Marshall,**[b,*] **Antonin Portelli,**[b] **J Tobias Tsang**[e] **and Oliver Witzel**[f]

[a] *Brookhaven National Laboratory, Upton, NY 11973, USA*

[b] *Higgs Centre for Theoretical Physics, School of Physics and Astronomy, The University of Edinburgh, James Clerk Maxwell Building, Peter Guthrie Tait Road, Edinburgh, EH9 3FD, UK*

[c] *Physics and Astronomy, University of Southampton, Southampton, SO17 1BJ, UK*

[d] *Theoretical Physics Department, CERN, 1211 Geneva 23, Switzerland*

[e] *CP3-Origins and IMADA, University of Southern Denmark, Campusvej 55, DK-5230 Odense M, Denmark*

[f] *Center for Particle Physics Siegen, Theoretische Physik 1, Naturwissenschaftlich-Technische Fakultät, Universität Siegen, 57068 Siegen, Germany*

E-mail: Michael.Marshall@ed.ac.uk

We present the status of our project to calculate $D \to \pi \ell \nu$, $D \to K \ell \nu$ and $D_s \to K \ell \nu$ semileptonic form factors using domain wall fermions for both heavy and light quarks. Our computations are performed using RBC/UKQCD's set of 2+1 flavour domain wall fermion and Iwasaki gauge field ensembles. We plan to calculate three-point functions covering the full, physically allowed kinematic range. Given that the signal decays faster than the noise, unambiguously and reliably extracting the ground state is critical for success. We include an analysis of operator diagonalisation within several possible 2×2 operator bases and find an admixture of gauged fixed wall and $\mathbb{Z}(2)$ wall sources to be acceptable at both zero and non-zero momentum. Initial results for semileptonic form factors are presented for first ensembles.

The 38th International Symposium on Lattice Field Theory, LATTICE2021 26th-30th July, 2021 Zoom/Gather@Massachusetts Institute of Technology

*Speaker

PoS(LATTICE2021)416

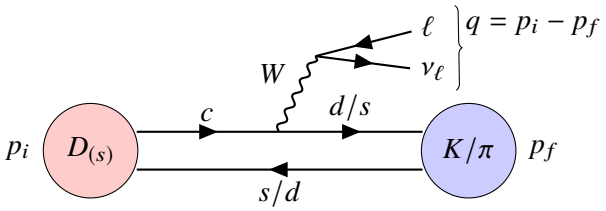

Figure 1: Tree-level semileptonic decay of an initial pseudoscalar $D_{(s)}$ meson (with momentum p_i) to a final pseudoscalar K or π meson (momentum p_f). Momentum $q = p_i - p_f$ is transferred to the final-state $\ell\nu$ pair.

1. Introduction

The six-quark model and the Cabibbo-Kobayashi-Maskawa (CKM) matrix was first proposed as a "very interesting and elegant" [1–3] mechanism to explain CP-violation. Half a century later, the model still stands and the study of flavour-changing processes has become the field of flavour physics.

Precise experimental measurements from charm factories such as CLEO-c and BESIII and bottom-factories such as Belle, Belle II, BaBar and LHCb continue to test the Standard Model and the unitarity of the CKM matrix to ever greater precision. Hints of potential new physics exist but to resolve them requires increased precision in theoretical prediction and experimental results.

The aim of this work is to perform lattice computations of the matrix elements of exclusive semileptonic meson decays involving $c \to d$ and $c \to s$ flavour transitions (fig 1). We use this to extract the q^2-dependence of the relevant form factors over the entire physically allowed kinematic range.

Experimental results for semileptonic meson decays quote products of form factors and CKM matrix elements. Recent HFLAV values for D-meson decays [4–6] give $\left|V_{cs} f_+^{D\to K}(0)\right| = 0.7133(68)$ and $\left|V_{cd} f_+^{D\to\pi}(0)\right| = 0.1400(33)$, i.e. errors of 1% and 2.4% respectively. By combining the experimental results with our lattice form factors, we aim to extract $|V_{cd}|$ and $|V_{cs}|$ which will allow us to test the unitarity of the CKM matrix in the Standard Model.

Our immediate goal is to perform the form factor determination to percent-level accuracy in order to be commensurate with the experimental results. Our approach complements the existing literature by performing the computation entirely with domain wall fermions. For the charm quark we utilise the discretisation employed in [7], using a stout-smeared [8] Möbius [9] action. The light and strange quarks are simulated with the Shamir [10–14] kernel.

2. Point-wall diagonalisation study

In order to extract form factors with the smallest possible variance, we seek methods to reliably eliminate excited state contamination from the two- and three-point functions we use on the earliest possible timeslice. Our earlier study of pseudoscalar-axial diagonalisation proved equivocal [15]. In this study we examined whether linear combinations of correlators constructed from point and wall operators could be used.

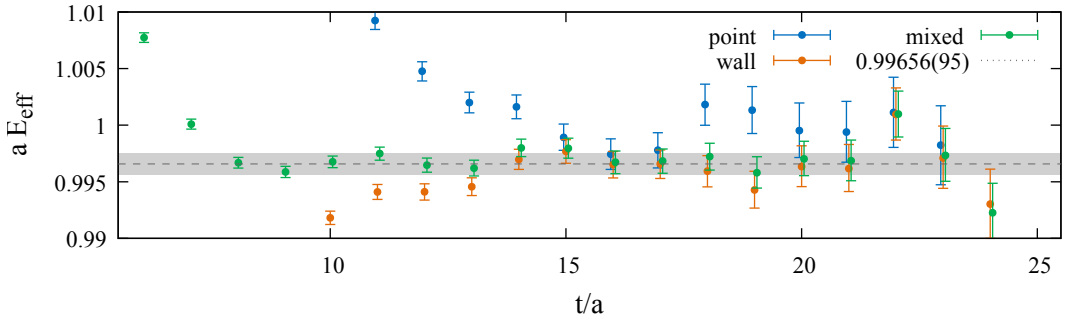

Figure 2: Effective mass plot $aE_{\text{eff}}(t) = \cosh^{-1}(C(t-1) + C(t+1)/2C(t))$ for a D-meson $C^{(2)}_{\text{mixed}}(t, \mathbf{0})$ constructed from C_{PP} and C_{WP} using overlap coefficients extracted from combined fit on timeslices [7, 17]. The green data points are obtained for an angle of $\theta = -\pi/4$. As expected, this choice leads to a significant reduction in excited state contamination. The grey dashed line (grey band) is the prior published result (variance) [7] (Table VI, $am_h = 0.58$)

We label pseudoscalar mesons $|P_i, n\rangle$ where P_i labels the initial or final meson (D, D_s, K or π), $n = 0$ labels ground and $n > 0$ label excited states. We use $|\Omega\rangle$ to denote the vacuum. When labelling an operator (and anything derived from an operator), the subscript $i \equiv$ initial and $f \equiv$ final also includes $P \equiv$ point and $W \equiv$ wall variants.

This study was performed on the RBC/UKQCD C1 ensemble [16]: $a^{-1} = 1.78\,\text{GeV}$; $L/a = 24$; $T/a = 64$; $m_\pi = 340$ MeV; $m_\pi L = 4.57$. This preliminary study uses a stout-smeared [8] Shamir [10–14] action for the charm, rather than stout-smeared Möbius [9] used in our production setup. This preliminary data set has 35 configurations, binning measurements from 16 timeslices on each.

2.1 Two-point diagonalisation study

We construct two-point correlation functions $C^{(2)}_{if}$ (with $i, f \in \{P, W\}$, i.e. point or wall) using interpolating operators $O = \bar{\psi}_2 \Gamma \psi_1$ with $\Gamma \in \{\gamma_5, \gamma_T\gamma_5\}$ appropriate for pseudoscalar mesons. Defining $A_{f,n} \equiv \langle\Omega|O_f|n\rangle$ and using the labels $i \equiv$ initial and $f \equiv$ final, the correlation function can be parameterised as

$$C^{(2)}_{if}(t, \mathbf{p}) \equiv \sum_{\mathbf{x}} e^{i\mathbf{p}\cdot\mathbf{x}} \left\langle O_f(t, \mathbf{x}) O_i^\dagger(0, \mathbf{0}) \right\rangle = \sum_n \frac{A_{f,n} A^*_{i,n}}{2E_n} \left(e^{-E_n t} \pm e^{-E_n (T-t)} \right). \tag{1}$$

Consideration of the ground and first excited state in (1) leads us to define a linear combination for a source mixing angle θ (where the first excited states are expected to cancel for $\theta = -\pi/4$)

$$C^{(2)}_{\text{mixed}}(\theta, t, \mathbf{p}) = \frac{\sin\theta}{A_{W,1}} C^{(2)}_{WP}(t, \mathbf{p}) + \frac{\cos\theta}{A_{P,1}} C^{(2)}_{PP}(t, \mathbf{p}), \tag{2}$$

where we extract the $A_{f,n}$ from simultaneous fits to the point and wall correlation functions.

We observe that the mixed correlator reaches a plateau around timeslice 8, much earlier than the underlying point and wall correlators (which plateau around timeslice 15), and the mass is compatible with prior published results [7] (Table VI, $am_h = 0.58$). Plateauing much earlier, the relative error of the mixed correlator is much smaller than that of the underlying correlators when they reach plateau. We conclude that excited state cancellations occur as expected.

2.2 Three-point diagonalisation study

Heavy-light/strange three-point functions with local current V_μ have the form (ignoring around-the-world effects and assuming P_i is located on timeslice 0)

$$C^{\mu}_{if}\left(\Delta T, t, \mathbf{p}_i \mathbf{p}_f\right) = \sum_{m,n=0}^{\infty} \frac{A_{f,m} A_{i,n}}{4 E_{f,m} E_{i,n}} \left\langle P_f\left(\mathbf{p}_f\right), m \middle| V^{\mu}(q^2) \middle| P_i\left(\mathbf{p}_i\right), n \right\rangle \mathrm{e}^{-\left(E_{i,n} - E_{f,m}\right)t} \, \mathrm{e}^{-E_{f,m}\Delta T} \,. \quad (3)$$

We construct two symmetric (with respect to the sink and source meson) double ratios, R^{μ}_1 and R^{μ}_2 [17, 18], which are designed to approach the renormalised ground state matrix element for $\Delta T \gg t \gg 0$, leaving the matrix element of the renormalised current

$$R^{\mu}_{\alpha}\left(\mathbf{p}_i, \mathbf{p}_f\right) = 2\sqrt{\frac{E_i E_f}{D_\alpha}} \sqrt{C^{\mu}_{if}\left(\mathbf{p}_i, \mathbf{p}_f\right) \, C^{\mu}_{fi}\left(\mathbf{p}_f, \mathbf{p}_i\right)} \approx Z_V \left\langle P_f\left(\mathbf{p}_f\right) \middle| V^{\mu}(q^2) \middle| P_i\left(\mathbf{p}_i\right) \right\rangle, \quad (4)$$

where $a \in \{1, 2\}$ and the denominator is: $D_1 = C^{(2)}_{ii}\left(\mathbf{p}_i\right) C^{(2)}_{ff}\left(\mathbf{p}_f\right) \Big/ \left(Z_{V\mathrm{h}} Z_{V\mathrm{l}}\right)$ (see section 3.2 for $Z_{V\mathrm{h}} \equiv Z_{V\,\text{heavy}}$ and $Z_{V\mathrm{l}} \equiv Z_{V\,\text{light/strange}}$); or $D_2 = C^{0}_{ii}\left(\mathbf{p}_i, \mathbf{p}_i\right) C^{0}_{ff}\left(\mathbf{p}_f, \mathbf{p}_f\right)$. We define mixed three-point functions (simplifying the notation and introducing arbitrary constants α, β, γ and δ)

$$C^{\mu}_{\substack{\text{source}\\\text{mixed},f}} = \alpha \, C^{\mu}_{\text{point},f} + \beta \, C^{\mu}_{\text{wall},f} \quad , \quad (5)$$

$$C^{\mu}_{\text{mixed}} = \gamma \, C^{\mu}_{\substack{\text{source}\\\text{mixed},\text{point}}} + \delta \, C^{\mu}_{\substack{\text{source}\\\text{mixed},\text{wall}}} . \quad (6)$$

We can show that if we introduce tunable mixing angles ϕ at sink and θ at source

$$\gamma = \frac{\cos\phi}{A^{(\text{point})}_{f,1}}, \qquad \delta = \frac{\sin\phi}{A^{(\text{wall})}_{f,1}}, \qquad \alpha = \frac{\cos\theta}{A^{(\text{point})}_{i,1}} \quad \text{and} \quad \beta = \frac{\sin\theta}{A^{(\text{wall})}_{i,1}}, \quad (7)$$

then we expect excited state cancellations. That is, near $\phi = \theta = -\pi/4$ the mixed three-point function approaches this form

$$C^{\mu}_{\text{mixed}} \approx \frac{\left(\gamma A^{(\text{point})}_{f,0} + \delta A^{(\text{wall})}_{f,0}\right)\left(\alpha A^{(\text{point})}_{i,0} + \beta A^{(\text{wall})}_{i,0}\right)}{4 E_f E_i} \left\langle P_f \middle| V^{\mu} \middle| P_i \right\rangle \mathrm{e}^{-\left(E_i - E_f\right)t} \, \mathrm{e}^{-E_f \Delta T}, \quad (8)$$

which is the exponential behaviour of the ground-state. We extract the $A^{(\text{point/wall})}_{f/i,1}$ from simultaneous fits to the point and wall correlation functions, $C^{(2)}_{PP}\left(t, \mathbf{p}\right)$ and $C^{(2)}_{WP}\left(t, \mathbf{p}\right)$. In the absence of exact knowledge of the numerical values of $A^{(\text{point/wall})}_{f/i,1}$, the parameters α, β, γ and δ can be tuned to optimise the excited state cancellation.

When we plot the effective mass of the source mixed correlation function (left panel, fig 3), the correlator is an interpolation between the point and wall sources. There is no obvious improvement as there was with the two-point source mixed correlation function. Tuning the mixing angle(s) makes little difference.

Similarly, when we plot the R_α ratios, we see no obvious improvement near $\phi = \theta \sim -\frac{\pi}{4}$. If a scan over all mixing angles is performed, we see that the optimal mixing angle (right panel fig 3) involves mostly the wall-source.

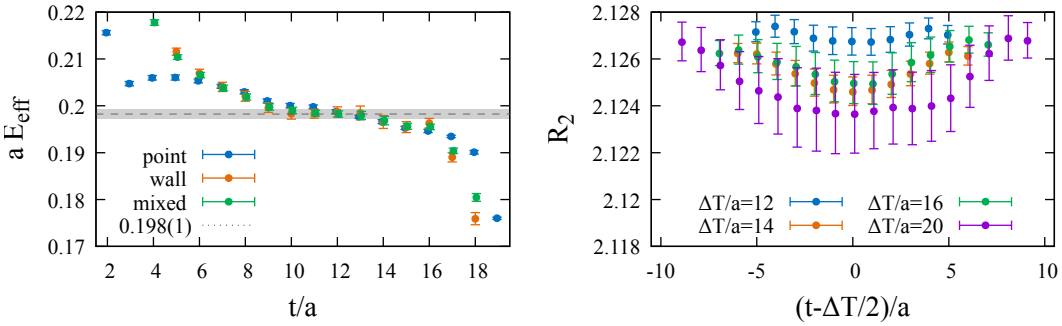

Figure 3: The (unphysical) transition $D_s\big|_{am_c=0.69} \to D_s\big|_{am_c=0.50}$. *Left:* $C^{\mu}_{\text{source mixed,point}}\left(\theta = -\frac{\pi}{4}\right)$, $\Delta T/a = 20$. Near the mid-point, the ground-state in (3) dominates, and the effective mass of the three-point function approximates the meson mass difference, 0.198(1) [7]. *Right:* Mixed R_2 ratio at $\theta = \phi \sim -80°$ (determined from a scan over mixing angles). We see agreement for multiple wall separations $\Delta T/a$ (except for $\Delta T/a = 12$). The statistical variance increases as the wall separation is increased.

3. Preliminary $D_{(s)} \to K/\pi\ \ell\nu$ data production

Data presented in this section were created on the RBC/UKQCD M1 ensemble [19, 20]: $a^{-1} = 2.38(1)$ GeV; $L/a = 32$; $T/a = 64$; $m_\pi = 300$ MeV; $m_\pi L = 4.08$ using a stout-smeared [8] Möbius [9] action for the charm, with Shamir [10–14] action for the light and strange quarks. This is the first ensemble from what will be our production data set, and the bare charm quark mass is chosen to be $am_h = 0.477$. We present results for 128 configurations, computing inversions on a single timeslice per configuration.

3.1 Fitting the two-point correlation function

In order to produce the mixed correlators defined in equations (2) and (8), we extract the overlap coefficients per (1) from simultaneous, two-state fits to $C^{(2)}_{PP}$ and $C^{(2)}_{WP}$ (see fig 4).

Fit results are stable and consistent over the scanned fit ranges, except where fit ranges start very early or very late. Prior results [7] (Table 6) bracket the values determined here: $am_D\big|_{am_h=0.50} = 0.8489(11)$ and $am_D\big|_{am_h=0.41} = 0.74931(91)$.

3.2 Extracting Z_V

Due to Lorentz invariance, the renormalised matrix element is parameterised in terms of the form factors f_+ and f_- as

$$Z_V \left\langle P_f\left(\mathbf{p}_f\right)\middle|V^{\mu}(\mathbf{q}^2)\middle|P_i\left(\mathbf{p}_i\right)\right\rangle = f_+^{P_iP_f}(q^2)\left(p_i + p_f\right)^{\mu} + f_-^{P_iP_f}(q^2)\left(p_i - p_f\right)^{\mu}. \tag{9}$$

Due to charge conservation, the form factor f_+ at vanishing momentum transfer is unity, i.e. $f_+^{P_iP_i} = 1$. Considering the rest frame where $p_i = p_f \implies p_i + p_f = (2E_i, \mathbf{0})$ and $p_i - p_f = 0$ we find (in the limit as $\Delta T \gg t \gg 0$)

$$Z_V = \frac{2E_i}{\langle P_i\left(\mathbf{0}\right)|V_0\left(\mathbf{0}\right)|P_i\left(\mathbf{0}\right)\rangle} \simeq \frac{C^{(2)}_{ii}\left(\Delta T, \mathbf{0}\right)}{C^{4,\text{bare}}_{ii}\left(\Delta T, t, \mathbf{0}, \mathbf{0}\right)}. \tag{10}$$

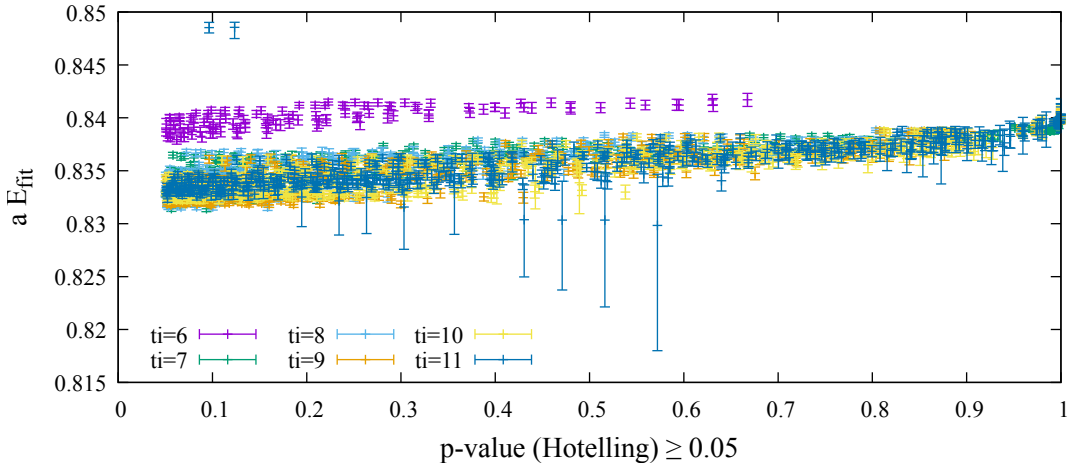

Figure 4: Fit results for $aE_D\big|_{am_h=0.477}$ extracted from simultaneous, two-state fits to $C^{(2)}_{PP}$ and $C^{(2)}_{WP}$ at $|\mathbf{n}|^2 = 2$, scanning over independent fit ranges for each correlator. The horizontal axis is the p-value of the fit using the Hotelling distribution and colour is used to indicate the initial fit time on $C^{(2)}_{PP}$ (all other labels suppressed).

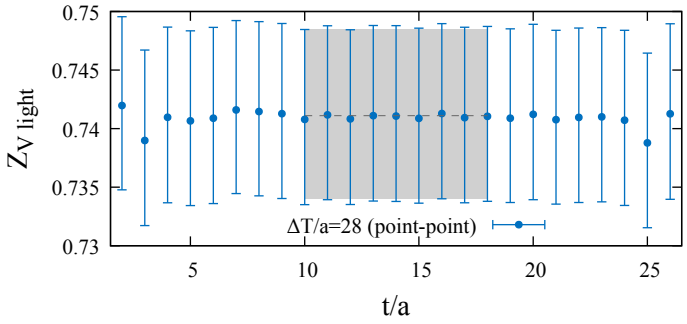

Figure 5: $Z^K_{V\,\text{light}}$ extracted from Kaon 2- and 3-point functions with $\Delta T/a = 28$. A correlated fit over $t/a \in [10, 18]$ (shaded region) yields $Z^K_V = 0.741(7)$, compatible with the published result 0.74563(13) [21].

We use this as a prescription to extract Z_V, emphasising that the denominator in (10) is the bare (unrenormalised) correlator, following [18]. Z_V is extracted by forming the ratio defined on the right hand side of equation (10) and fitting it to a constant in the region where excited state contributions are negligible (see fig 5).

We have a different action for the heavy vs the strange and light quark propagators and as a temporary measure we treat the mixed action bilinear using $Z_{V\,\text{mixed}} = \sqrt{Z_{V\,\text{heavy}} Z_{V\,\text{light/strange}}}$. However, in future we plan to use non-perturbative renormalisation [22] on the mixed action bilinear.

3.3 Three-point data

Our aim is to map out the q^2 dependence of the form factors over the entire physical kinematic range. In our setup, the heavier meson is always kept at rest and the integer momentum $\mathbf{n} = \mathbf{p}\, L/(2\pi)$

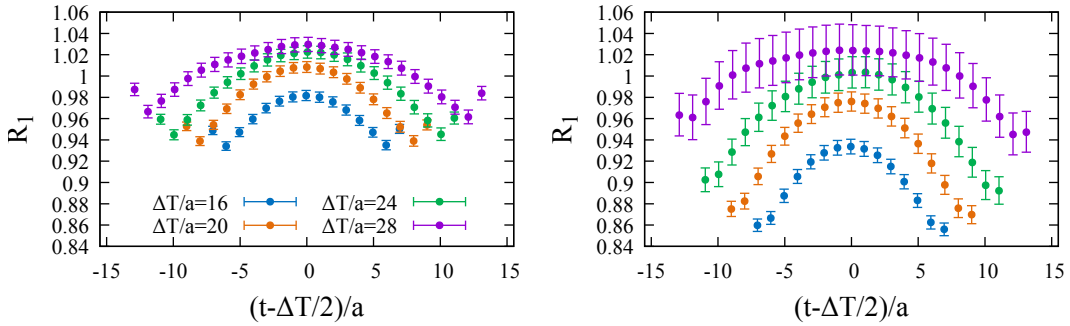

(a) $R_1^4\left(q^2_{\text{max}}\right), D_s \to K$ **(b)** $R_1^4\left(q^2_{\text{max}}\right), D \to \pi$

Figure 6: Temporal component of R_1 for $D_s \to K$ and $D \to \pi$ decays for $|\mathbf{n}|^2 = 0$, $V^0\left(q^2_{\text{max}}\right)$ (point source and point sink). Excited state contamination is clearly present for small $\Delta T/a$ (as evidenced by the lack of plateau and failure to agree with other source-sink separations). At larger $\Delta T/a$ the data overlap and we see a plateau, but it is not clear that excited states have been fully eliminated. A fit to multiple $\Delta T/a$ will likely be required to reliably obtain the asymptotic plateau with small error.

of the lighter meson labels the process. The momentum transfer to the lepton pair is $q = p_i - p_f$ (see fig 1), for which the physical range is $m_\ell^2 \leq q^2 \leq q^2_{\text{max}} = (M_{P_f} - M_{P_i})^2$. For $\mathbf{n} = \mathbf{0}$, $q^2 = q^2_{\text{max}}$ and as $|\mathbf{n}|^2$ increases we move down in q^2, reaching $q^2 \simeq 0$ for $|\mathbf{n}|^2 = 4$ on the $M1$ ensemble for the mesons of interest.

In order to assess their statistical properties, we produced both ratios defined in equation (4) for all three decays: $D_s \to K$, $D \to K$ and $D \to \pi$. The denominator for R_2 requires production of additional three-point correlators, making the R_2 ratio twice as expensive to calculate. We found that the results for R_1 and R_2 are consistent, with errors of the same magnitude. Due to the reduced cost of data production, we anticipate that we will only generate data for R_1 in the future. For this reason, only data for R_1 is shown in figures 6-9.

These proceedings show our methodology and give a flavour of the quality of our data produced to date. As we are still in the process of refining the analysis strategy, the data shown are preliminary.

3.3.1 Temporal component of R_1 at q^2_{max}

The $D_s \to K$ decay is a charm to light transition with a strange spectator, whereas the $D \to \pi$ decay has a light spectator. The light propagator on the lattice is noisier than the strange, resulting in smaller relative uncertainties in fig 6a compared with fig 6b.

There is clearly excited state contamination at small $\Delta T/a$, which appears much reduced at larger $\Delta T/a$ although not necessarily fully suppressed. As expected, errors grow quite distinctly with $\Delta T/a$. We would ideally like to use the statistically cleaner data from smaller $\Delta T/a$ in our analysis. This means we will need to model the excited state behaviour and include that in our fits for our full analysis – the double-ratios alone will not be sufficient to fully control the contamination from the excited states.

3.3.2 Spatial and temporal component of R_1 at non-zero momentum

Data have been produced across the physically allowable kinematic range. Results for spatial and temporal components of the vector current with one unit of momentum are shown in fig 7.

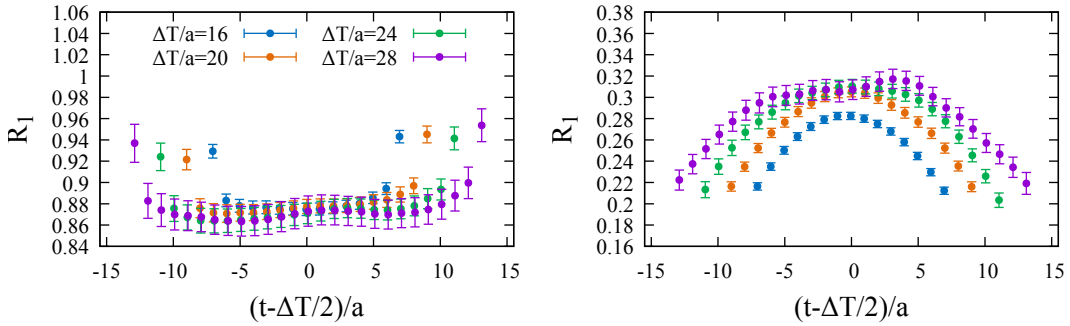

(a) $R_1^4\,(n^2 = 1)$ **(b)** $R_1^i\,(n^2 = 1)$

Figure 7: Temporal (fig 7a) and spatial (fig 7b) components of R_1 for $D_s \to K$ decays for $|\mathbf{n}|^2 = 1$, (point-point).

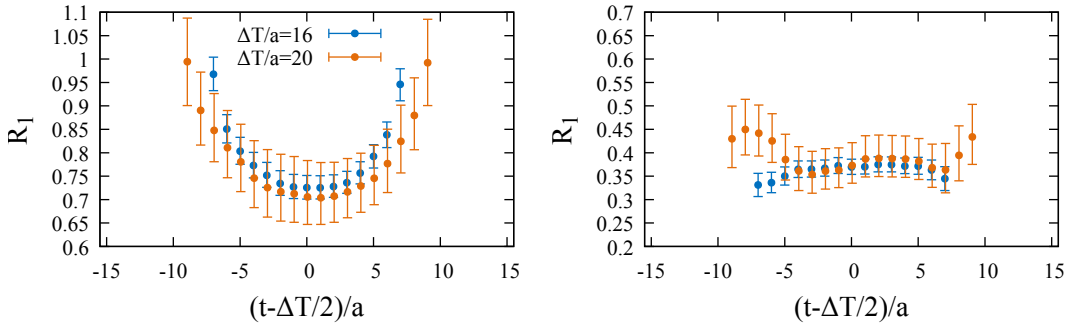

(a) $R_1^4\,(\sim q_0)$ **(b)** $R_1^i\,(\sim q_0)$

Figure 8: Temporal (fig 8a) and spatial (fig 8b) components of R_1 for $D_s \to K$ decays near q_0 (i.e. $|\mathbf{n}|^2 = 4$), (point-point).

The errors are larger than for q^2_{max}, but still under control. Even though all but the smallest source-sink separations reach a consistent plateau value within statistical uncertainties, an analysis taking the excited states into account will allow us to quantify residual excited state contamination and thereby utilise the most precise data points whilst maintaining control over systematic uncertainties.

3.3.3 Data for R_1 near $q^2 = 0$

Near the maximum recoil point $q^2 = 0$, the final state meson carries several units of momentum, resulting in larger statistical uncertainties. For visibility, we have removed the very noisy data points corresponding to source-sink separations of $\Delta T/a \geq 24$ from figure 8.

We are currently investigating whether data should be produced over a smaller range of $\Delta T/a$ in finer increments as part of our fitting strategy evaluation. We might also increase statistics.

3.3.4 Fitting strategy

Figures 6-8 present data for the ratio R_1 for point sources and sinks. In addition, we also produced data with wall sources and sinks as well as the mixed cases. Figure 9 shows this data at

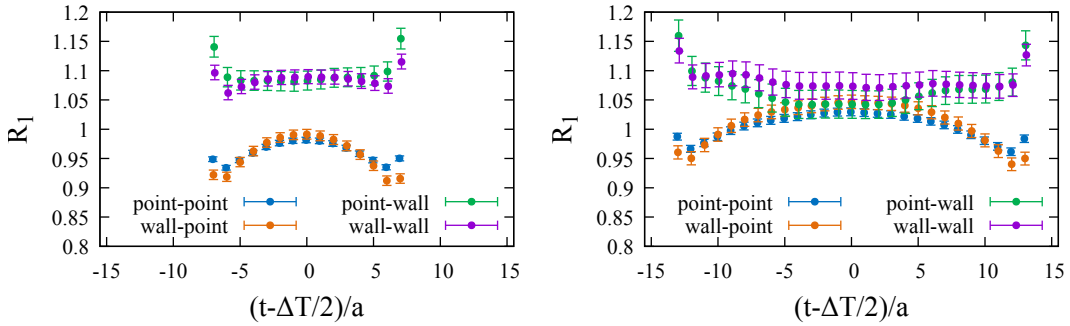

(a) $R_1^4\left(q^2_{\text{max}}\right)$ $(\Delta T/a = 16)$ **(b)** $R_1^4\left(q^2_{\text{max}}\right)$ $(\Delta T/a = 28)$

Figure 9: Point(wall)-sink temporal components of R_1 for $D_s \to K$ approach plateau from below(above). This is consistent across source-sink separations, e.g.: $\Delta T/a = 16$ (fig 9a) and $\Delta T/a = 28$ (fig 9b).

fixed source-sink separation for the temporal component of R_1 at zero recoil (q^2_{max}). We observe the qualitatively different approach to the plateau of the wall-sink data, which approaches the plateau from above, while the point data approaches the plateau from below. We intend to utilise the various features of our data set by simultaneously fitting the different operator choices and multiple source-sink separations.

Based on the data we have, we expect to be able to extract the form factors over the entire physical kinematic range.

4. Summary and Outlook

We performed a study on point-wall diagonalisation as a method for reducing excited state contamination. The method works very well for two-point functions, however, extending this to the three-point functions is still work in progress.

We have produced two- and three-point correlation functions for $D_{(s)} \to K/\pi$ semileptonic decays on our first ensemble, which we present here. After examining the three-point correlation function data on this first ensemble, we conclude that we will need to use wall separations which do not fully eliminate excited state contamination (even when analysed using double-ratio methods). We will, therefore, simultaneously fit correlator data from multiple wall separations, giving greater control over excited state contamination.

Having both point and wall correlation function data, with differing approaches to plateau, gives us extra control over excited states. We can include the point and wall correlation functions separately in our simultaneous fits and/or use a rotated basis for our fits. Due to noise issues with the wall sink data, we may use a one-sided diagonalisation at the source only for the three-point correlation function – but this is to be determined and work is ongoing to finalise our analysis.

Since the lattice conference, we have optimised our performance on DiRAC's new Tursa NVidia A100 GPU-based supercomputer and we have produced data for a second ensemble.

The target result is the q^2-dependence of the $D_{(s)} \to K/\pi$ form factors over the entire physical q^2 range, and results from our first ensemble indicate that percent-scale errors are achievable.

Acknowledgments

Kind thanks to the RBC/UKQCD collaboration for many invaluable discussions and helpful suggestions. Results presented here were produced using Grid [23] and Hadrons [24].

This work used the DiRAC Extreme Scaling service at the University of Edinburgh, operated by the Edinburgh Parallel Computing Centre on behalf of the STFC DiRAC HPC Facility (https://www.dirac.ac.uk). This equipment was funded by BEIS capital funding via STFC capital grant ST/R00238X/1 and STFC DiRAC Operations grant ST/R001006/1. DiRAC is part of the National e-Infrastructure.

P.B. has been supported in part by the U.S. Department of Energy, Office of Science, Office of Nuclear Physics under the Contract No. DE-SC-0012704 (BNL). P.B. has also received support from the Royal Society Wolfson Research Merit award WM/60035. L.D.D. is supported by the U.K. Science and Technology Facility Council (STFC) grant ST/P000630/1. F.E. and A.P. are supported in part by UK STFC grant ST/P000630/1. F.E. and A.P. also received funding from the European Research Council (ERC) under the European Union's Horizon 2020 research and innovation programme under grant agreement No 757646 and A.P. additionally under grant agreement No 813942. A.J. and J.F. acknowledge funding from STFC consolidated grant ST/P000711/1 and A.J. from ST/T000775/1. M.M. gratefully acknowledges support from the STFC in the form of a fully funded PhD studentship. J.T.T.: the project leading to this application has received funding from the European Union's Horizon 2020 research and innovation programme under the Marie Skłodowska-Curie grant agreement No 894103.

References

[1] M. Kobayashi, *CP violation and flavor mixing (Nobel lecture)*, *ChemPhysChem* **10** (2009) 1706.

[2] N. Cabibbo, *Unitary symmetry and leptonic decays*, *Physical Review Letters* **10** (1963) 531.

[3] M. Kobayashi and T. Maskawa, *CP-violation in the renormalizable theory of weak interaction*, *Progress of theoretical physics* **49** (1973) 652.

[4] HFLAV collaboration, *Averages of b-hadron, c-hadron, and τ-lepton properties as of 2018*, *The European physical journal. C, Particles and fields* **81** (2021) 226 [1909.12524].

[5] M. Ablikim, M. Achasov, S. Ahmed, X. Ai, O. Albayrak, M. Albrecht et al., *Analysis of $D^+ \to \bar{K}^0 e^+ \nu_e$ and $D^+ \to \pi^0 e^+ \nu_e$ semileptonic decays*, *Physical Review D* **96** (2017) [1703.09084].

[6] M. Ablikim, M. Achasov, S. Ahmed, M. Albrecht, M. Alekseev, A. Amoroso et al., *Study of the $D^0 \to K^- \mu^+ \nu_\mu$ dynamics and test of lepton flavor universality with $D^0 \to K^- \ell^+ \nu_\ell$ decays*, *Physical Review Letters* **122** (2019) [1810.03127].

[7] RBC/UKQCD collaboration, *SU(3)-breaking ratios for $D_{(s)}$ and $B_{(s)}$ mesons*, 1812.08791.

[8] C. Morningstar and M.J. Peardon, *Analytic smearing of SU(3) link variables in lattice QCD*, *Physical Review D* **69** (2004) 054501 [hep-lat/0311018].

[9] R.C. Brower, H. Neff and K. Orginos, *The Möbius domain wall fermion algorithm*, *Comput. Phys. Commun.* **220** (2017) 1 [1206.5214].

[10] D.B. Kaplan, *A method for simulating chiral fermions on the lattice*, *Physics Letters B* **288** (1992) 342 [hep-lat/9206013].

[11] Y. Shamir, *Chiral fermions from lattice boundaries*, *Nuclear Physics B* **406** (1993) 90 [hep-lat/9303005].

[12] V. Furman and Y. Shamir, *Axial symmetries in lattice QCD with Kaplan fermions*, *Nuclear Physics B* **439** (1995) 54 [hep-lat/9405004].

[13] T. Blum and A. Soni, *QCD with domain wall quarks*, *Physical Review D* **56** (1997) 174 [hep-lat/9611030].

[14] T. Blum and A. Soni, *Domain wall quarks and kaon weak matrix elements*, *Physical Review Letters* **79** (1997) 3595 [hep-lat/9706023].

[15] P. Boyle, F. Erben, M. Marshall, F. Ó hÓgáin, A. Portelli and J.T. Tsang, *An exploratory study of heavy-light semileptonic form factors using distillation*, *PoS* **363** (2020) 169 [1912.07563].

[16] Y. Aoki et al., *Continuum limit of B_K from 2+1 flavor domain wall QCD*, *Phys. Rev. D* **84** (2011) 014503 [1012.4178].

[17] RBC-UKQCD collaboration, *Hadronic form factors in lattice QCD at small and vanishing momentum transfer*, *Journal of High Energy Physics* **2007** (2007) 016 [hep-lat/0703005].

[18] P.A. Boyle, J.M. Flynn, N. Garron, A. Jüttner, C.T. Sachrajda, K. Sivalingam et al., *The kaon semileptonic form factor with near physical domain wall quarks*, *Journal of High Energy Physics* **2013** (2013) [1305.7217].

[19] RBC, UKQCD collaboration, *Continuum limit physics from 2+1 flavor domain wall QCD*, *Physics Review D* **83** (2011) 074508 [1011.0892].

[20] RBC-UKQCD collaboration, *Physical results from 2+1 flavor domain wall QCD and SU(2) chiral perturbation theory*, *Physics Review D* **78** (2008) 114509 [0804.0473].

[21] RBC/UKQCD collaboration, *The kaon semileptonic form factor in $N_f = 2 + 1$ domain wall lattice QCD with physical light quark masses*, *Journal of High Energy Physics* **06** (2015) 164 [1504.01692].

[22] P. Boyle, L.D. Debbio and A. Khamseh, *A massive momentum-subtraction scheme*, *Phys. Rev. D* **95** (2017) 054505 [1611.06908].

[23] P. Boyle, A. Yamaguchi, G. Cossu and A. Portelli, *Grid: A next generation data parallel C++ QCD library*, 1512.03487.

[24] A. Portelli, N. Asmussen, P. Boyle, F. Erben, V. Gülpers, R. Hodgson et al., *aportelli/hadrons: Hadrons*, 10, 2020. 10.5281/zenodo.4063666.